17th Brazilian Congress of Thermal Sciences and Engineering
November 25th-28th, 2018, Águas de Lindóia, SP, Brazil

ENCIT-2018-0719
POROUS AND NON-POROUS MICROSTRUCTURED SURFACES FOR BOILING HEAT TRANSFER APPLICATIONS

Leonardo Lachi Manetti[1], leonardo.manetti@unesp.br
Igor Seicho Kiyomura[1], igor.kiyomura@unesp.br
Elaine Maria Cardoso[1], elaine.cardoso@unesp.br
[1]UNESP – São Paulo State University, Post-Graduation Program in Mechanical Engineering, Av. Brasil, 56, 15385-000, Ilha Solteira, SP, Brazil.

Abstract. *In the last decades, the need for more efficient and compact heat exchangers, especially in microelectronics, and products with high thermal load has been motivating the research on new technics for increasing the boiling heat transfer. The heating surface can be modified by using random micro- or nano-size cavities, porous structure, or protrusions that enlarge the effective area for heat transfer. In this context, we analyze modified heating surfaces consisting of micro-fin array surfaces or metal foams of nickel (Ni), copper (Cu) or stainless steel (SS). All surfaces were submitted to metallographic (stereoscopic and scanning electron microscopy), DI-water droplet dynamic, wettability and thermal image analyses to obtain the wall-temperature profile. It was possible to find out details about the surfaces morphology such as porous size, porous per inches (PPI), and porosity. Furthermore, the DI-water droplet dynamic showed that the stainless steel porous surface has a superhydrophilic behavior; the others surfaces tested, even the open cell metal foams, showed a non-wetting behavior. The infrared thermography analysis showed that the DI-water droplets on Cu foam surface and SS foam surface heat faster than that on the plain surface; however, in the Ni foam surface, the droplet is slowly heated. The thermal behavior is a function of the wettability and absorption behavior of the surfaces (capillary wicking behavior).*

Keywords: *heating surface, porous, foam, micro-fin surface, pool boiling.*

1. INTRODUCTION

Efficient thermal management solutions are crucial to maintaining the electronic devices within the operating temperature limits (Leong et al., 2017). The thermal systems with two-phase change such as pool and flow boiling, jet impingement, and spray cooling have been used as a way of reaching the power dissipation needed by these devices.

Several combinations of liquid-surface have been studied in pool boiling as summarized by Shojaeian and Kosar (2015). One promising way to enhance the heat transfer coefficient (HTC) and the critical heat flux (CHF) is modifying the heating surface morphology. According to Hendricks et al. (2010) the heating surface can be modified by using three factors: (i) existence of random micro- or nano-size crevices and surface irregularities for bubble nucleation, (ii) porous surface structure that allows fluid inflow to keep nucleation sites active and, (iii) surface protrusions that enlarge the boiling surface area. The modification methods/techniques used to modify the surfaces are classified as follows:

- Coating process (homogeneous/heterogeneous): consists of material addition/deposition on a heating surface by using chemical vapor deposition, sputtering, dripping, nanofluid boiling process, sintered particles, and welding carbon/metal foams or mesh.
- Machining techniques and chemicals processes: based on material removal/corrosion by using precision machining as computer numeric control (CNC), electric discharge machining, laser, oxidation, chemical etching, micro/nano electromechanical system (MEMS/NEMS) technique (photolithography technique, reactive ion etching/deep reactive ion etching) (Kim et al., 2015).

Moreover, pool boiling predictive models as Rohsenow (1952), Li et al. (2014) and Kiyomura et al. (2017) show that the liquid-surface interaction mainly the wettability - measured by the contact static angle - and the sensible heat transfer influence the boiling performance.

In this context, we characterize modified heating surfaces obtained by two different methods and submit them to metallographic (stereoscopic and scanning electron microscopy), wettability, wickability and thermal image analyses in order to study their performance on pool boiling applications.

2. METHODOLOGY

The modified heating surfaces were obtained by two methods: coating and micro-milling process. The first one consists of metal foams of nickel (Ni), copper (Cu) or stainless steel (SS). The second one consists of micro-fin array

surfaces. We used the following methods to characterize all surfaces: (i) optical images using a stereo microscope – Zeiss® SteREO Discovery.V8; (ii) scanning electron microscopy (SEM) by using an EVO LS15 Zeiss®; (iii) droplet dynamic of a 10 µl DI-water droplet and surface wettability by using a high-speed camera (Fig. a); (iv) wickability by using a capillary tube (1 mm) within DI-water by using a high-speed camera (Fig. 1b) according to Ahn et al. (2012) and Rahman et al. (2014); and, (iv) thermal analysis of a 10 µl DI-water droplet by recording pictures with an IR camera FLIR T440 SC (Fig. 2).

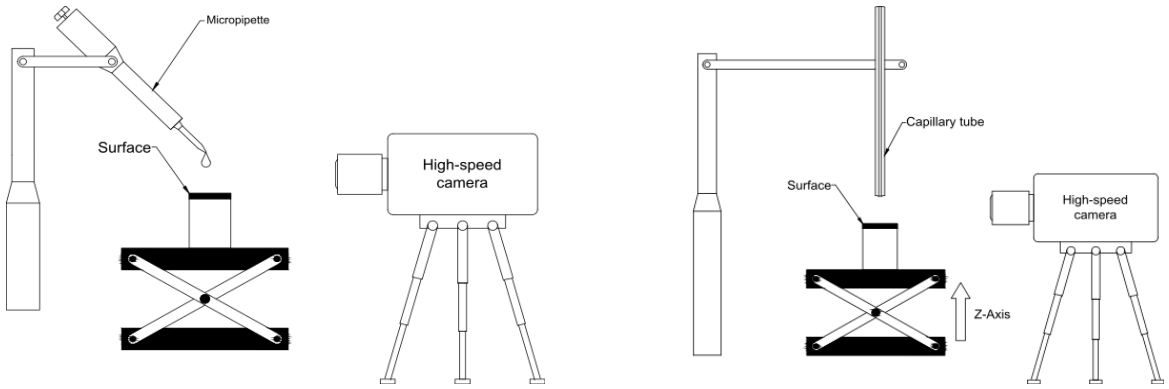

Figure 1. Schematic layout of wettability analysis (a) and wickability analysis (b).

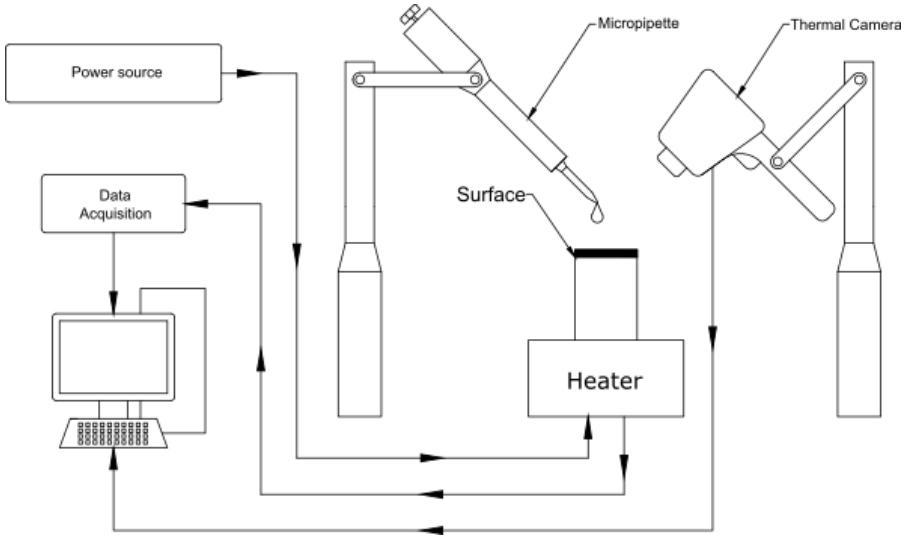

Figure 2. Experimental apparatus for the thermography analysis.

2.1 Porous surfaces

We purchased the porous surfaces from Nanoshel®. Two of them are open cell metal foam fabricated by using metal casting or deposition in a cellular preform as detailed by Ashby et al. (2000). The other one is a porous surface without open cell structure fabricated by using sintering of metal powders as detailed by Banhart (2001) and Singh and Bhatnagar (2017). According to Yang et al. (2010), porosity and numbers of pores per inch (PPI) are the two parameters that influence the heat transfer. These parameters are measurable quantities as showed by Athreya et al. (2002) and Zhu et al. (2014). In order to perform the PPI measurements, firstly, one sample of each foam was characterized in the stereoscopic; thus, seven lines in each direction were traced and the number of porous in which intercepted lines were counted; so, an average of each direction line were calculated and also, the average of the two direction yields the PPI of the open cell metal foam. We obtained the porosity by weighting seven samples with the same area in an analytical balance and comparing the foam weight with that of a solid sample with equivalent volume ($16 \times 16 \times 3$ mm³). Moreover, optical and electronic images were used for measuring the surfaces porous and fibers diameters.

2.2 Micro-fin array surfaces

Squares micro-fins of different length scales (*i.e.*, height, diameter, and inter-fin space) were uniformly spaced on the plain copper surface. The inter-fin space had the same value, 250 µm, for all surfaces in order to control the effective roughness, *r*, defined as the ratio of the true area in contact with the liquid to the projected area, as showed by

Chu et al. (2012) and Dong (2014). The square-micro pillar arrays were etched on a plain copper surface through micro-milling process by using CNC precision machining.

3. RESULTS

3.1 Stereoscopic and SEM images

Table 1 shows the optical and scanning electron microscopy (SEM) images of porous surfaces used in this study.

Table 1. Stereoscopic and SEM images of porous surfaces.

Sterescopic top surface image	Sterescopic side surface image	SEM top surface image
Cu foam		
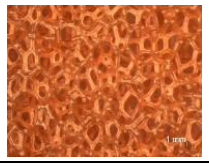	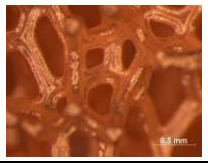	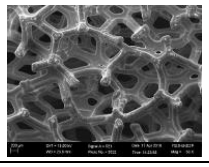
Ni foam		
	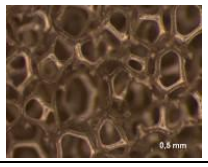	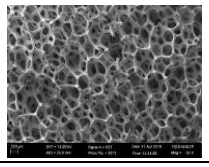
SS foam		
	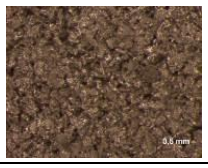	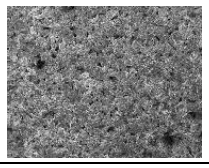

For Cu and Ni open cell metal foam, the average PPI value was 31.75 and 62.72, respectively. The PPI measurement for SS foam was not carried out due to the absence of cell structure.

Table 2 shows the average porosity and pore diameter for copper, nickel, and stainless steel foams.

Table 2. Porosity measurements for metal foams.

	Weight [kg ×10^{-3}]	Foam Density [kg/m³]	Relative Density [1] [%]	Porosity	Pore diameter (mm)	Fiber diameter (mm)
Cu	0.697 ± 0.009	908.1 ± 11.7	10.14 ± 0.13	0899 ± 0.001	0.49 ± 0.14	0.21 ± 0.03
Ni	0.106 ± 0.004	138.02 ± 5.8	1.55 ± 0.06	0.984 ± 0.001	0.27 ± 0.07	0.07 ± 0.01
SS	3.168 ± 0.010	4125.0 ± 12.7	53.92 ± 0.17	0.460 ± 0.002	0.04 ± 0.02	-

(1)Pure material density: ρ_{Cu} = 8960 kg/m³; ρ_{Ni} = 8900 kg/m³; ρ_{SS} = 7650 kg/m³.

The open cell metal foams have a high porosity (> 80%) and their pore and fiber diameter decrease as the PPI increase. The SS foam has lower porosity than the other ones however its porous diameter is tiny.

Table 3 shows the optical, scanning electron microscopy (SEM) images and, the length scales of the micro-fin array surfaces.

Table 3. Stereoscopic and SEM images of the micro-fin array surfaces.

Top surface image	Side surface image	SEM top surface image	Height [µm]	Diameter [µm]	Inter-fin space [µm]	Effective roughness[1], *r*
Micro-fin n.1						
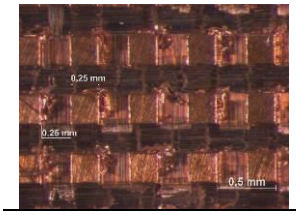	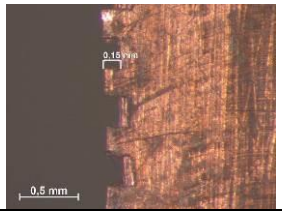	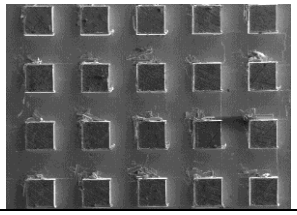	150	250	250	1.60

Top surface image	Side surface image	SEM top surface image	Height [μm]	Diameter [μm]	Inter-fin space [μm]	Effective roughness[1], *r*
Micro-fin n.2						
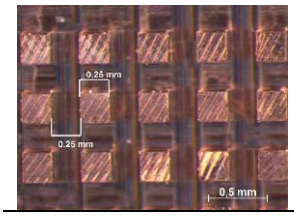	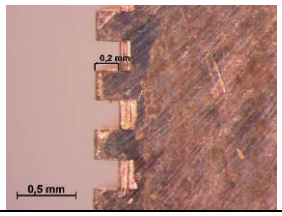	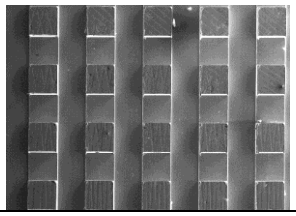	200	250	250	1.80
Micro-fin n.3						
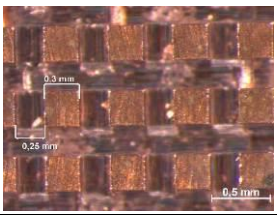	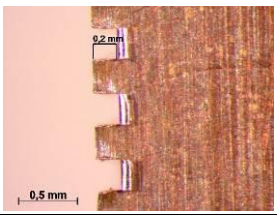	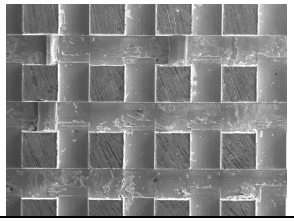	200	300	250	1.79

[1] $r = 1 + \left[4DH/(S+D)^2\right]$

The micro-fin array has a good symmetry; the effective roughness, *r*, increases as the diameter or the height of micro-fins changes, being the height effect more pronounceable.

3.2 Droplet dynamic, wettability, and wickability

Table 4 shows the DI-water droplet dynamic and surface wettability for all surfaces. In addition to the modified surfaces, we also tested a plain surface (corresponding to a copper surface with R_a = 0.05 μm) as a reference surface.

Table 4. DI-water droplet dynamic for all surfaces tested in this study.

Plain surface				
				
0 ms	6 ms	12 ms	15 ms	Stabilized, 450 ms
Cu foam				
				
0 ms	6 ms	12 ms	15 ms	Stabilized at 300 ms
Ni foam				
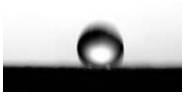	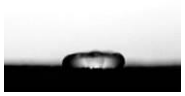			
0 ms	6 ms	12 ms	15 ms	Stabilized at 550 ms
SS foam				
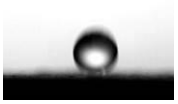				
0 ms	6 ms	12 ms	15 ms	70 ms
				
Spreading at 258 ms	206 ms	166 ms	148 ms	112 ms

Micro-fin n.1				
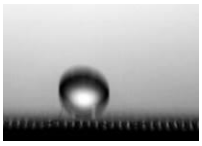	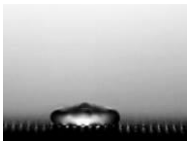	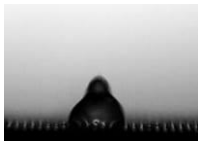	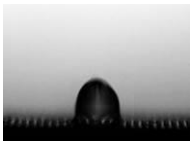	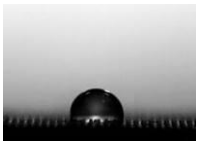
0 ms	6 ms	12 ms	15 ms	Stabilized at 550 ms
Micro-fin n.2				
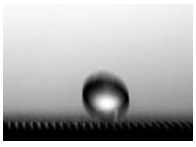	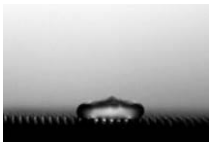	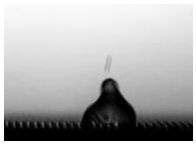		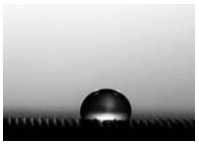
0 ms	6 ms	12 ms	15 ms	Stabilized at 550 ms
Micro-fin n.3				
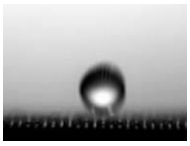	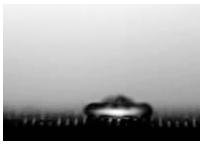			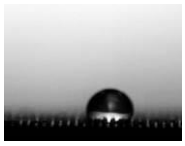
0 ms	6 ms	12 ms	15 ms	Stabilized at 550 ms

The plain, high porosity foams and micro-fins showed low wetting behavior. The SS foam also showed a low wetting behavior in the initial time; however, the pore absorbed the droplet. This effect is due to the lowest pore diameters in this surface - approximately 5 times lower than the Cu or Ni foams and the micro spacing in the micro-fins array surface. The small pore size increases the capillary effect. In order to understand this phenomenon, we carried out a wickability analysis on theses surfaces.

Table 5 shows the wickability of plain surface, micro-fin n.2, Ni foam and SS foam. The others surfaces: micro-fin n.1 and n.3, as well as, Cu foam presented similar behavior to the plain surface, *i.e.*, these surfaces do not show a capillary wicking behavior as can be observed at the meniscus of the capillary tube during the test time. In contrast, the SS foam absorbed the liquid from the capillary tube, corroborating with the wicking surface hypothesis.

Table 5. Wickability of surfaces by using DI-water in a capillary tube.

Plain surface				
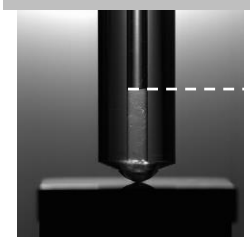	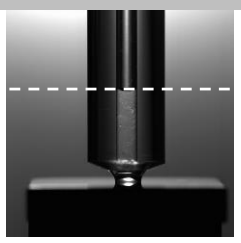	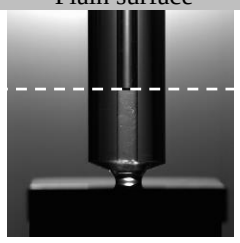	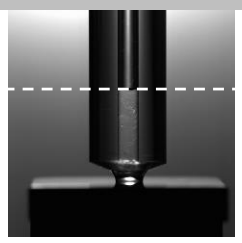	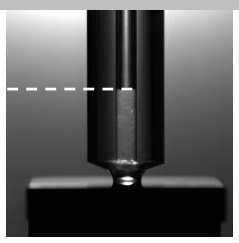
0 ms	10 ms	50 ms	100 ms	500 ms
Micro-fin n.2				
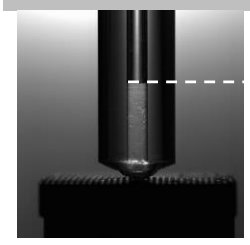	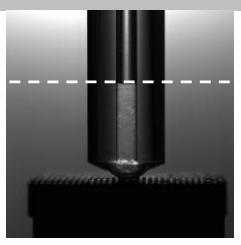	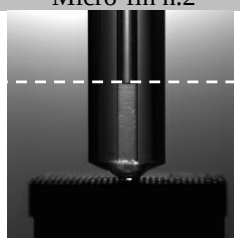	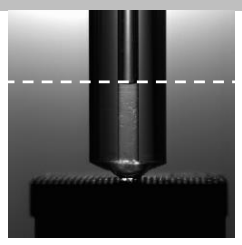	
0 ms	10 ms	50 ms	100 ms	500 ms
Ni foam				
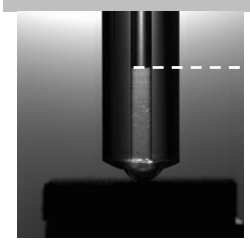	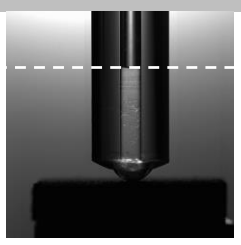	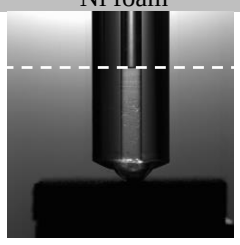	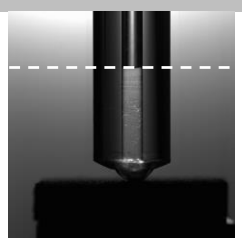	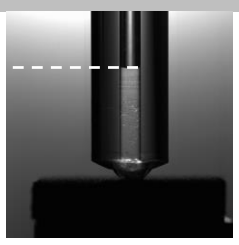
0 ms	10 ms	50 ms	100 ms	500 ms

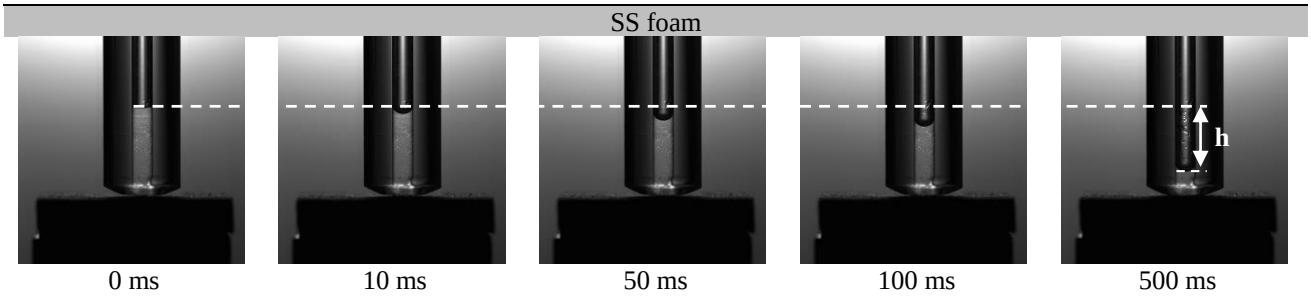

3.3 Thermal analysis

Figure 3 shows the thermal analysis for the Cu, Ni, SS porous surfaces and micro-fins surfaces. In addition, a plain copper surface was also tested. The temperature data corresponds to the average value in the region of interest, ROI (red circle), obtained by using the FLIR® ResearchIR software.

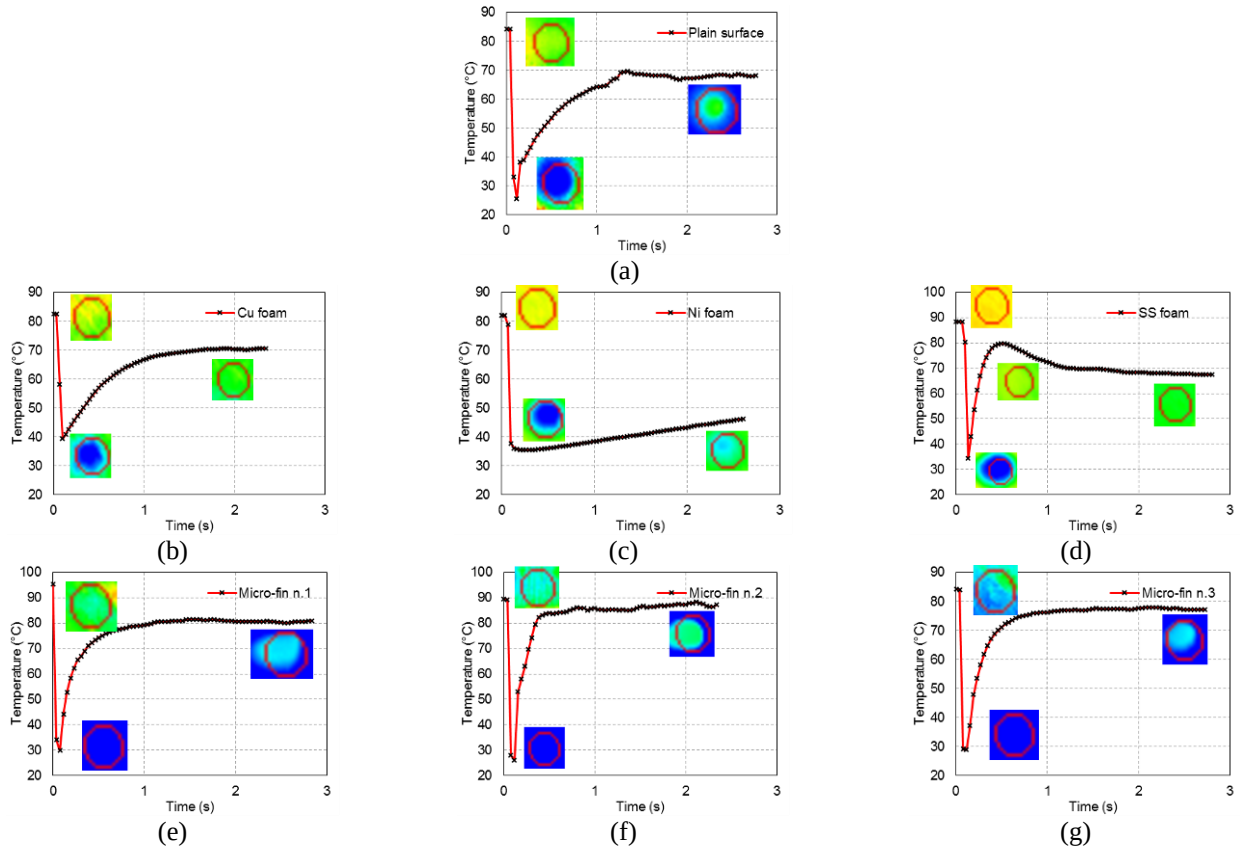

Figure 3. Wall-temperature profile as function of time using DI-water droplet on plain polished surface (a); Cu foam (b); Ni foam (c); SS foam (d), and micro-fins n.1 (e); n.2 (f); n.3 (g).

At instant time t = 0, the infrared camera emissivity was adjusted to identify the temperature close to the thermocouple temperature located on the surface; at the instant time t > 0, at the moment of the droplet impact on the surface, the emissivity was adjusted to capture the droplet temperature. One may observe that the micro-fins surfaces transfer heat quickly to the DI-water droplet in comparison with the plain and the high porosity foams (Cu and Ni foams). The SS foam has an initial behavior similar to the micro-fins surfaces; however, as the SS foam is able to absorb the droplet (as shown in the section 3.2) the IR camera will record again the surface temperature.

4. CONCLUSION

The modified surfaces characterization allows the understanding of the surface morphology such as porous size, PPI, porosity and effective roughness. The DI-water droplet dynamic shows that the stainless steel porous surface is able to absorb and spread the droplet; the others surfaces, including Cu and Ni foams, shows a low wetting behavior. The thermal analysis shows that the DI-water droplets on Cu foam, micro-fins surface and the SS foam surface heat faster than those on the plain copper surface, being the SS foam the fastest. The surface thermal behavior is a function

of the surface morphology and its surface wettability and capillary wicking (fluid-surface interaction). Based on the analysis, these surfaces have contact angles close to 90° or less than 20°, being able to increase the HTC as explained by Phan et al. (2009). Moreover, the larger contact area with liquid as compared to the plain surface can increase the active nucleation sites (Zhao, 2012; Dong et al., 2014). In addition, the capillary wicking through the surface - observed for the SS foam - is reported as the main effect to the critical heat flux enhancement (CHF) (Ahn, 2012; Cao et al., 2018).

5. ACKNOWLEDGEMENTS

The authors are grateful for the financial support from the PPGEM – UNESP/FEIS, from CAPES, from CNPq (grant number 458702/2014-5) and from FAPESP (grants number 2013/15431-7 and 2017/13813-0). The authors also extend their gratitude to Prof. Dr. Gherhardt Ribastki (Heat Transfer Research Group) and to Prof. Alessandro Roger Rodrigues (Lab. de Processos de Fabricação – LAMAFE) from EESC/University of São Paulo.

6. REFERENCES

Ahn, H. S., Park, G., Kim, J. M., Kim, J. and Kim, M. H., 2012. "The effect of water absorption on critical heat flux enhancement during pool boiling." *Experimental Thermal and Fluid Science*, Vol. 42, pp. 187-195.

Ashby, M. F., Evans, T., Fleck, N. A., Hutchinson, J. W., Wadley, H. N. G. and Gibson, L. J., 2000. *Metal foams: a design guide*. Elsevier.

Athreya, B., Mahajan, R. and Sett, S., 2002. "Pool boiling of FC-72 over metal foams: effect of foam orientation and geometry" In *Proceeding of 8th AIAA/ASME Joint Thermophysics and Heat Transfer Conference*. St Louis, Missouri, USA.

Banhart, J., 2001. "Manufacture, characterization and application of cellular metals and metal foams." *Progress in materials science* Vol. 46, n.6, pp. 559-632.

Cao Z., Liu B., Preger, C., Wu, Z,. Zhang, Y., Wang, X., Messing, M. E., Deppert, K., Wei, J. and Sundén, B., 2018. "Pool boiling heat transfer of FC-72 on pin-fin silicon surfaces with nanoparticle deposition". *Int. J. Heat Mass Transf.* Vol. 126, pp.1019–1033.

Chu, K-H., Enright, R., and Wang, E. N., 2012. "Structured surfaces for enhanced pool boiling heat transfer." *Applied Physics Letters*, Vol. 100, n. 24, p. 241603.

Dong, L., Xiaojun Q. and Ping C., 2014. "An experimental investigation of enhanced pool boiling heat transfer from surfaces with micro/nano-structures." *International Journal of Heat and Mass Transfer*, Vol. 71, pp. 189-196.

Hendricks, T. J., Krishnan, S., Choi, C., Chang, C. H. and Paul, B., 2010. "Enhancement of pool-boiling heat transfer using nanostructured surfaces on aluminum and copper". *International Journal of Heat and Mass Transfer*, Vol. 53, n. 15-16, pp. 3357-3365.

Kim, D. E., Yu, D. I., Jerng, D. W., Kim, M. H. and Ahn, H. S., 2015. "Review of boiling heat transfer enhancement on micro/nanostructured surfaces". *Experimental Thermal and Fluid Science*, Vol. 66, pp. 173-196.

Kiyomura, I. S., Mogaji, T. S., Manetti, L. L. and Cardoso, E. M., 2017. "A predictive model for confined and unconfined nucleate boiling heat transfer coefficient". *Applied Thermal Engineering*, Vol. 127, pp. 1274-1284.

Leong, K. C.,Ho, J. Y. and Wong, K. K., 2017. "A critical review of pool and flow boiling heat transfer of dielectric fluids on enhanced surfaces." *Applied Thermal Engineering*, Vol. 112, pp. 999-1019.

Li, Y-Y., Chen, Y-J., Liu, Z-H., 2014. "A uniform correlation for predicting pool boiling heat transfer on plane surface with surface characteristics effect". International Journal of Heat and Mass Transfer, Vol. 77, pp. 809-817.

Rahman, M. M., Olceroglu, E. and McCarthy, M., 2014. "Role of wickability on the critical heat flux of structured superhydrophilic surfaces". *Langmuir*, Vol. 30, n. 37, pp. 11225-11234.

Rohsenow, W. M., 1952. "A method of correlating heat transfer data for surface boiling of liquids. *Transactions of ASME – Journal of Heat Transfer*, Vol. 74, pp. 969-976.

Phan. H.T., Caney, N., Marty P., Colasson, S. and Gavillet, J., 2009. "Surface wettability control by nanocoating: The effects on pool boiling heat transfer and nucleation mechanism". *Int. J. Heat Mass Transf.*, Vol. 52, pp. 5459–5471.

Shojaeian, M. and Koşar, A., 2015. "Pool boiling and flow boiling on micro-and nanostructured surfaces." *Experimental Thermal and Fluid Science*, Vol. 63, pp; 45-73.

Shweta, S. and Bhatnagar, N., 2018. "A survey of fabrication and application of metallic foams (1925–2017)." *Journal of Porous Materials*, Vol. 25, n-2, pp. 537-554.

Yang, Y., Ji, X. and Xu, J., 2010. "Pool boiling heat transfer on copper foam covers with water as working fluid". *International Journal of Thermal Sciences*, Vol. 49, n. 7, pp. 1227-1237.

Zhao, C.Y., 2012. "Review on thermal transport in high porosity cellular metal foams with open cells". *Int. J. Heat Mass Transf.* Vol. 55 pp. 3618–3632.

Zhu, Y., Hu, H., Sun, S., and Ding, G., 2014. "Heat transfer measurements and correlation of refrigerant flow boiling in tube filled with copper foam". *International Journal of Refrigeration*, Vol. 38, pp. 215-226.

7. RESPONSIBILITY NOTICE

The authors are the only responsible for the printed material included in this paper.